Steel and Composite Structures, *Vol. 34, No. 1* (*2020*) *1-15*
DOI: https://doi.org/10.12989/scs.2020.34.1.001

Experimental and numerical investigations on remaining strengths of damaged parabolic steel tubular arches

Yonghui Huang[1a], Airong Liu[*1], Yong-Lin Pi[1,2b], Mark A. Bradford[2c] and Jiyang Fu[1d]

[1]*Guangzhou University-Tamkang University Joint Research Center for Engineering Structure Disaster Prevention and Control*, *Guangzhou University*, *Guangzhou 510006*, *China*
[2]*Centre for Infrastructure Engineering and Safety* (*CIES*), *School of Civil and Environmental Engineering*, *The University of New South Wales*, *Sydney*, *NSW 2052*, *Australia*

(*Received January 15, 2019, Revised October 29, 2019, Accepted December 15, 2019*)

Abstract. This paper presents experimental and numerical studies on effects of local damages on the in-plane elastic-plastic buckling and strength of a fixed parabolic steel tubular arch under a vertical load distributed uniformly over its span, which have not been reported in the literature hitherto. The in-plane structural behaviour and strength of ten specimens with different local damages are investigated experimentally. A finite element (FE) model for damaged steel tubular arches is established and is validated by the test results. The FE model is then used to conduct parametric studies on effects of the damage location, depth and length on the strength of steel arches. The experimental results and FE parametric studies show that effects of damages at the arch end on the strength of the arch are more significant than those of damages at other locations of the arch, and that effects of the damage depth on the strength of arches are most significant among those of the damage length. It is also found that the failure modes of a damaged steel tubular arch are much related to its initial geometric imperfections. The experimental results and extensive FE results show that when the effective cross-section considering local damages is used in calculating the modified slenderness of arches, the column bucking curve *b* in GB50017 or Eurocode3 can be used for assessing the remaining in-plane strength of locally damaged parabolic steel tubular arches under uniform compression. Furthermore, a useful interaction equation for assessing the remaining in-plane strength of damaged steel tubular arches that are subjected to the combined bending and axial compression is also proposed based on the validated FE models. It is shown that the proposed interaction equation can provide lower bound assessments for the remaining strength of damaged arches under in-plane general loading.

Keywords: local damage; strength; steel arch; experimental investigation; remaining strength; finite element analysis (FEA)

1. Introduction

Parabolic arches are widely used in long-span structures such as bridges because of their high-efficient in-plane load-carrying capacity, especially under a full-span uniformly distributed vertical load which produces nominal uniform compression in the arch rib. Steel structures are often exposed to the environment having water and oxygen, which may cause local damages to the steel and subsequently lead to unavoidable strength reduction (Rahgozar *et al*. 2010). Investigations of the in-plane buckling and strength of steel arches have mainly focused on arches without damages. Pi and Trahair (1999), Bradford and Pi (2004), Pi *et al*. (Pi and Bradford 2004, Pi *et al*. 2008) investigated the in-plane strength of pin-ended and fixed circular steel I-section arches, and developed interaction equations for their in-plane strength design. It was found that the modified slenderness of a steel arch, which is related to the in-plane elastic buckling of the arch and the yield load of the cross-section, is an important parameter in formulation of design equations. Liu *et al*. (2017) investigated the buckling behaviour of fixed circular arches subjected to an in-plane central concentrated load which produces combined nonuniform axial compressive and bending actions. Dou *et al*. (2018) studied the in-plane buckling behaviour and proposed design equations of steel tubular truss arches. Yang *et al*. (2019) studied the nonlinear in-plane buckling of fixed shallow functionally graded grapheme reinforced composite arches subjected to mechanical and thermal loading. In experimental research aspect, Sakimoto *et al*. (1979) carried out tests to investigate the strength of circular and parabolic steel arches. Dou *et al*. (2015) conducted experimental investigation into flexural-torsional ultimate resistance of steel circular arches. Guo *et al*. (2016) performed experimental and numerical investigations of the in-plane strength of pin-ended circular steel arches having a welded I-section and proposed an interaction equation for the in-plane strength of arches. The results provided in these investigations are all about the in-plane behaviour of steel

*Corresponding author, Professor,
E-mail: liuar@gzhu.edu.cn
[a] Associate Professor, E-mail: huangyh@gzhu.edu.cn
[b] Professor, E-mail: y.pi@unsw.edu.au; y.pi@gzhu.edu.cn
[c] Professor, E-mail: m.bradford@unsw.edu.au
[d] Professor, E-mail: jiyangfu@gzhu.edu.cn

ISSN: 1229-9367 (Print), 1598-6233 (Online)

arches without damages.

When a steel arch is locally damaged, its strength may be reduced by the local damage. However, little research about the strengths of the locally damaged steel arches has been reported in the literature hitherto. Investigations of effects of damages caused by corrosion on the steel structures have been focused on straight girders or plates. Mateus and Witz (1998) used a FE analysis and a uniform thickness reduction approach to formulate a quasi-random thickness surface model to study the post-buckling of corroded steel plates. Rahgozar (2009) established corrosion decay models based on corrosion locations and studied effects of corrosion on the remaining capacity of steel beams. Sharifi and Paik (2011) developed a probabilistic model for the strength of steel-box girders on the basis of an analytic formula that considers time-dependent strength degradation related to corrosion. Appuhamy *et al.* (2011) discussed the feasibility of establishing an accurate analytical method to predict the residual strength of a corroded steel member with lesser number of measuring points, and they (Appuhamy *et al.* 2013) also investigated effects of severe corrosion on the remaining seismic strength of existing steel bridges using finite element (FE) analyses. Kaita *et al.* (2012) proposed an approach to calculate the remaining yield and tensile strength by using a concept of representative effective thickness. Rahbar-Ranji (2013) found that the aspect ratio of the plate, the average thickness diminution, the standard deviation of thickness diminution and the amount of corrosion loss reduce the buckling strength of the corroded plates. Kim *et al.* (2013) conducted shear loading tests on five plate girder specimens with different corrosion heights and mean corrosion depths of a corroded web, and the critical shear buckling loads and shear buckling strengths were analyzed. Ahn *et al.* (2013) evaluated the residual shear strengths and shear failure modes of a web panel with local corrosion by using a FE analysis and the results were compared with results obtained from a theoretical equation and design specifications. Silva *et al.* (2013) developed two approaches to model the corrosion surface and to evaluate the strength of steel plate components and a total of 3575 corroded plate surface geometries by Monte Carlo simulation for different degrees of degradation, location and ages were investigated. Kainuma *et al.* (2015) created a three-dimensional FE model of a surface corroded orthotropic steel deck to examine the stress level dependence on the corrosion conditions and the results confirmed that surface corrosion may result in a high stress concentration and irregular stress distributions.

Although studies of effects of damages on the steel girders and plates caused by corrosion have been extensive, investigations of effects of local damages on the strength of steel arches are rare, while the local damage is a common problem in many steel arch bridges (Huang 2010). To ensure the safety of the damaged steel arches, it is necessary to assess their remaining strengths.

This paper, therefore, is focused on experimental and numerical investigations of effects of local damages on the in-plane strength of fixed parabolic steel tubular arches, which are often used in the engineering practice. The in-plane strengths of ten specimens with different local damages are investigated experimentally. A FE model is developed and validated using the test results, and it is then used to carry out extensive investigation of effects of various parameters such as the damage location, length and depth and the initial geometric imperfections on the remaining in-plane strength of damaged steel tubular arches with fixed ends. The experimental and FE results are used to develop equations for assessing the remaining strength of fixed parabolic steel tubular arches having local damages. Equations for assessing remaining strengths of damaged parabolic arches under uniform compression and under combined bending and axial compression are proposed.

2. Experimental program

2.1 Test specimens

Ten steel tubular arch specimens having local damages (Fig. 1) were prepared and tested, which were fabricated from hot-rolled seamless tubes in two steps. At first, damages with different lengths and depths at different locations are cut uniformly around the outer surface of straight hot-rolled seamless tubes by a high precision cutting machine. The straight tubes are then curved to parabolic arches by cold-bending methods. The diameter and thickness of the undamaged steel tubes are D = 95 mm and t_s = 8.0 mm, and the span and rise of the arches are L = 3.6 m and f = 0.9 m, respectively.

Three damage parameters: (1) the damage location (at the left arch end or arch crown); (2) the damage length (100 mm, 200 mm and 300 mm); (3) the damage depth (1.0 mm, 2.0 mm and 3.0 mm) are considered in fabrication of the damaged arch specimens. The damage location, length and depth of the 10 specimens are shown in Table 1, where the specimens are labeled as ST-8-X-Y-Z with ST denoting the steel tube, 8 the thickness of the undamaged tube, X, Y, Z the damage location, length and depth, respectively.

2.2 Geometric imperfections of specimens

Before testing, the initial in-plane geometric imperfections of the specimens were measured at nine stations with equal intervals along the axis of arch specimens and the measured results are shown in Fig. 2.

It can be seen that the in-plane geometric imperfections vary significantly. For example, the arch specimen ST-8-A-200-1.0 (the red curve in Fig. 2(a)) has approximately symmetric initial imperfections, the specimen ST-8-A-200-2.0 (the blue curve in Fig. 2(a)) has approximately antisymmetric initial imperfections, and the specimen ST-8 almost has no initial imperfections (the black curve in

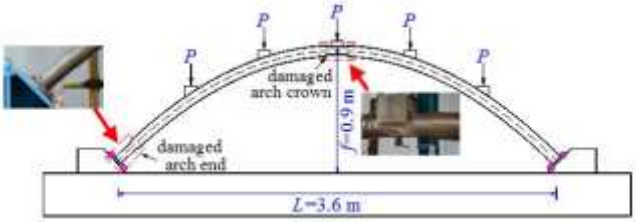

Fig. 1 The schematic of the test model

Table 1 Details of the specimens

No.	Specimen label	Damage location	Damage length (mm)	Damage depth (mm)
1	ST-8	--	0	0
2	ST-8-A-200-1.0	Left arch end	200	1.0
3	ST-8-A-200-2.0		200	2.0
4	ST-8-A-200-3.0		200	3.0
5	ST-8-A-100-3.0		100	3.0
6	ST-8-A-300-3.0		300	3.0
7	ST-8-D-200-2.0	Arch crown	200	2.0
8	ST-8-D-200-3.0		200	3.0
9	ST-8-D-100-3.0		100	3.0
10	ST-8-D-300-3.0		300	3.0

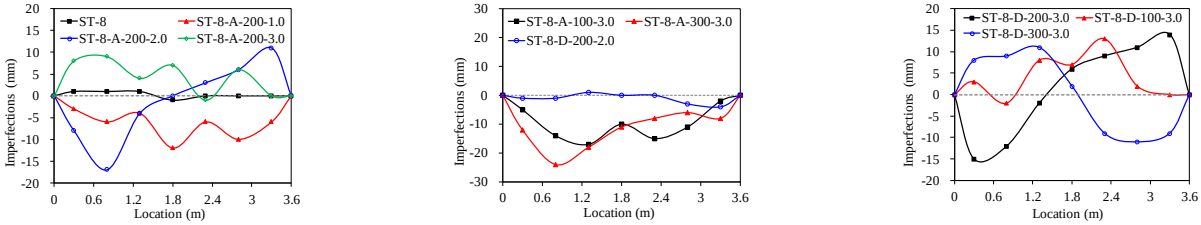

(a) Specimens 1-4 (b) Specimens 5-7 (c) Specimens 8-10

Fig. 2 Measured geometric initial imperfections

Fig. 2(a)). The initial geometric imperfections may have significant effects on the strength of the damaged steel arches.

In addition, the residual stresses may also affect the strength of steel arches. The residual stresses in the cold-

curved steel arches consist of two parts (Hadjoannou *et al*. 2011): the manufacturing and cold curving residual stresses. It has been shown that cold curving residual stresses have little effects on the strength of steel arches (Pi and Trahair 1999, Hadjoannou *et al*. 2011). Hence, cold curving residual stresses are not considered in this investigation. Because the manufacturing residual stresses of hot-rolled tubular sections are available in the literature, the residual stresses reported in Lin and Guo (2009) are used in this investigation.

2.3 Material properties

The steel of the tube is Q345. Three steel coupons having a length of 273 mm cut from the steel tubes were tested to determine the material properties of the steel and the results are listed in Table 2. The average yield strength (σ_y), ultimate strength (σ_u), elastic modulus (E), Poisson's ratio and elongation rate of the steel are 375.2 MPa, 542.0 MPa, 191,000 MPa, 0.292 and 26.3%, respectively.

The stress – strain curves of the three steel coupons are shown in Fig. 3. It can be seen that after yield, the modulus of the steel becomes zero until the strain reaches 0.022 when the strain hardening starts.

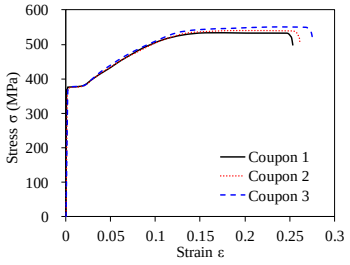

Fig. 3 Stress-strain curves for steel

Table 2 Mechanical properties of Q345 steel

Coupon	Young's modulus (MPa)	Yield stress (MPa)	Ultimate strength (MPa)	Poisson's ratio	Elongation rate (%)
1	2.00×10^5	375.1	533.8	0.305	25.4
2	1.91×10^5	368.3	541.0	0.295	26.1
3	1.82×10^5	382.2	551.1	0.276	27.5
Average	1.91×10^5	375.2	542.0	0.292	26.3

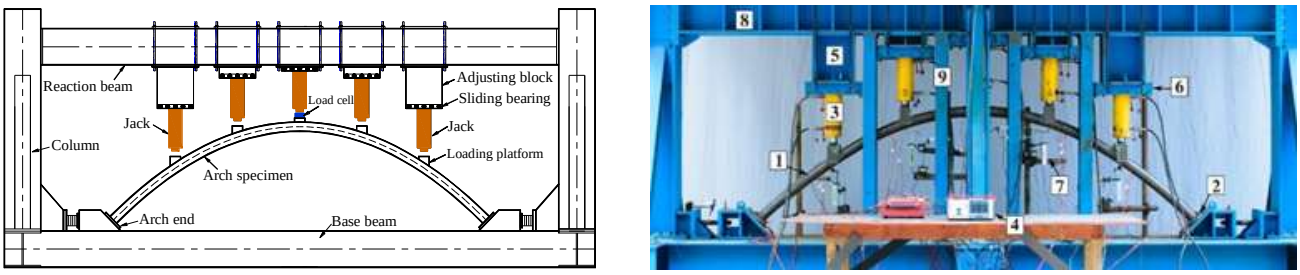

(a) Loading application scheme (b) Test setup

Fig. 4 Loading scheme and test setup (1. Arch, 2. Arch end, 3. Hydraulic jack, 4. Data logger, 5. Adjusting block, 6. Sliding bearing, 7. LVDT, 8. Reaction beam, 9. Lateral bracing)

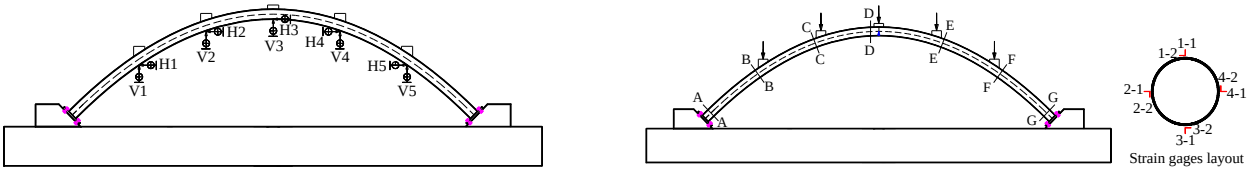

(a) Displacement measurement points (b) Strain measurement point

Fig. 5 Layout of displacement and strain measurement point

2.4 Test setup

The test rig was designed to apply the in-plane load to the arch specimens and to allow the arch specimen to deform in the plane of loading freely, while the out-of-plane deformations are fully prevented. The scheme of the test rig is shown in Fig. 4.

The test rig consists of a base beam, a reaction beam, two columns and lateral braces. A five-point vertical loads were applied at $L/6$, $L/3$, $L/2$, $2L/3$, $5L/6$ points of the arch rib to simulate the vertical uniform load (Fig. 4(a)), where L is the span of the arch specimen. The loading system consists of a reaction beam, five 500kN hydraulic jacks controlled by an oil pump, sliding bearings and load cells. The load was applied through hydraulic jacks and the reaction beam, and load cells were used to control the loading. To guarantee that the reaction beam does not restrain the longitudinal movement of the specimen during loading, oiled sliding bearings with almost no friction are placed between the jacks and reaction beam (Liu *et al.* 2015) as shown in Fig. 4(a). The hydraulic jacks and load cells are calibrated before each test. To prevent the arch specimen from the lateral deformations, four lateral bracings were placed at each side of the arch specimen (Fig. 4(b)). The sliding bearings were also installed between the lateral braces and the arch, so that the in-plane deformations were not restrained by the lateral braces.

2.5 Test procedures

An oil pump was used to apply the equal symmetric vertical loads through the five jacks to the arch specimen simultaneously. The data for the load, strain and displacement were recorded in real-time. When the strength of a specimen was reached, the load cell readings started to drop indicating the load started to decrease until the specimen finally failed.

2.6 Measurements

To capture the displacements and strains of specimens in real time, the vertical and horizontal LVDTs (linear variable differential transformer) were installed on the bottom of the cross-section at the loading points as shown in Fig. 5(a), where V and H indicate the vertical and horizontal LVDTs respectively, while rectangular strain-gauges rosettes were installed on the top, bottom and both sides of the cross-sections at seven locations i.e. A-A to G-G as shown in Fig. 5(b).

The strain gauges along the arch axis and in the transverse direction are denoted as n-1 and n-2 respectively, where n is the number of strain measurement point. All LVDTs, strain gauges and load cells were connected to a TDS-530 data logger to guarantee synchronization of data collections.

3. Experimental results and discussion

3.1 Failure mode

The test results showed that the failure of specimens is either in an asymmetric mode or in a symmetric mode. The typical failure modes are shown in Fig. 6 for specimens 3 and 7.

It can be seen that specimen 3 fails in an asymmetric elastic-plastic buckling mode (Fig. 6(a)) and the specimen 7 fails in a symmetric elastic-plastic buckling mode (Fig. 6(b)).

The deformation curves of all 10 specimens recorded at their failure are shown in Fig. 7 and the corresponding failure modes and initial geometric imperfections are listed

(a) Specimen 3 (asymmetric mode) (b) Specimen 7 (symmetric mode)

Fig. 6 Failure modes

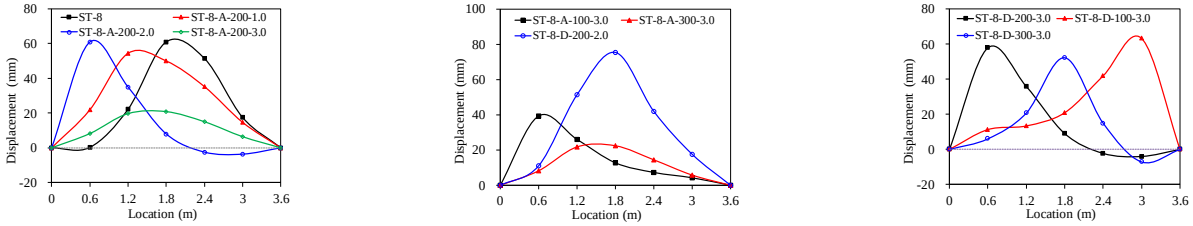

(a) Specimens 1-4 (b) Specimens 5-7 (c) Specimens 8-10

Fig. 7 Test deformation curves

Table 3 Test and FE failure modes

No.	Specimen label	Initial imperfection shape	FE failure mode	Test failure mode
1	ST-8	symmetric	symmetric	symmetric
2	ST-8-A-200-1.0	symmetric	symmetric	symmetric
3	ST-8-A-200-2.0	asymmetric	asymmetric	asymmetric
4	ST-8-A-200-3.0	symmetric	symmetric	symmetric
5	ST-8-A-100-3.0	symmetric	symmetric	symmetric
6	ST-8-A-300-3.0	symmetric	symmetric	symmetric
7	ST-8-D-200-2.0	symmetric	symmetric	symmetric
8	ST-8-D-200-3.0	asymmetric	asymmetric	asymmetric
9	ST-8-D-100-3.0	symmetric	symmetric	symmetric
10	ST-8-D-300-3.0	asymmetric	asymmetric	asymmetric

in Table 3. It is noted that in Fig. 7 and other figures of this paper, positive displacement indicates the point deformed downwards, while the negative displacement indicates the point deformed upwards.

It can be seen from Fig. 7 and Table 3 that the failure mode of a damaged steel arch much depends on the shape and magnitude of initial geometric imperfections of the arch. The arches having asymmetric initial geometric imperfections (Fig. 2 and Table 3) failed in an asymmetric mode (Fig. 7 and Table 3). The arches having symmetric initial geometric imperfections (Fig. 2 and Table 3) failed in a symmetric mode (Fig. 7 and Table 3). This indicates that initial geometric imperfections are indeed one of the major factors for the elastic-plastic buckling failure mode of a damaged steel tubular arch.

3.2 Displacement - Load curves

The typical displacement vs. load (*v-P*) curves of the specimen ST-8 with no damage recorded by the five vertical

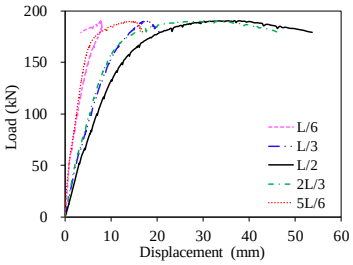

Fig. 8 Displacement-load curves of the specimen ST-8

LVDTs (V1-V5 in Fig. 5) are shown in Fig. 8.

Because the parabolic arch under a uniform vertical load is nominally subjected to axial uniform compression, the curves are initially linear until the onset of yielding at the top of the arch crown, and after that, a further increase of the load produced both axial compressive and bending actions in the arch specimen leading to the development of plastic deformations and gradual spreading of the plastic

zone. The plastic deformations reduce the compressive and bending stiffness of the arch significantly and the *v-P* curves become nonlinear and so the vertical displacements increase rapidly in association with a decrease of the slope of the *v-P* curves until the maximum load carrying capacity of the arch is reached. After this, the strength of the arch decreases in association with a further increase of the displacement and the slopes of the *v-P* curves become negative. The directions of the displacements along the arch length indicate that the arch failed in a symmetric mode.

The *v-P* curves of the five arch specimens having damages at their left end are shown in Fig. 9. It can be observed that for the arch specimens having the same damage length of 200 mm (Figs. 9(a)-(c)), the strength decreases with an increase of the damage depth. For arch specimens with the same damage depth of 3 mm (Figs. 9(c)-(e)), the strength decreases with an increase of the damage length.

The *v-P* curves of the four arch specimens having damages at their crown are shown in Fig. 10. Again, it can be observed that for arch specimens having the same damage length of 200 mm (Figs. 10(a)-(b)), the strength decreases with an increase of the damage depth. For arch specimens with the same damage depth of 3 mm (Fig.10(b)-(e)), the strength decreases with an increase of the damage length. The onset of yielding occurs at the top of the arch specimen crown.

3.3 Stress-load curves

The typical axial stress vs. load (σ- *P*) curves are shown in Fig. 11 for specimen 6 having the largest damage length

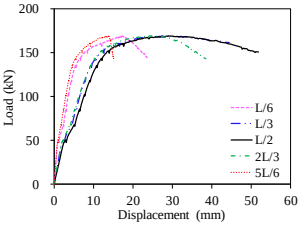

(a) ST-8-A-200-1.0

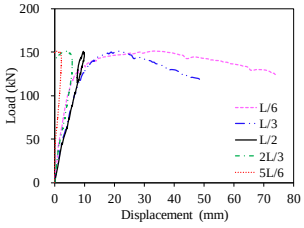

(b) ST-8-A-200-2.0

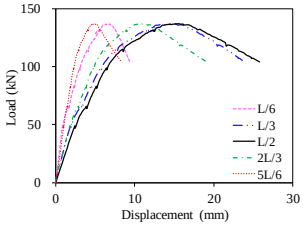

(c) ST-8-A-200-3.0

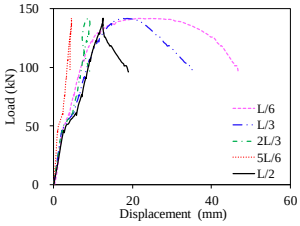

(d) ST-8-A-100-3.0

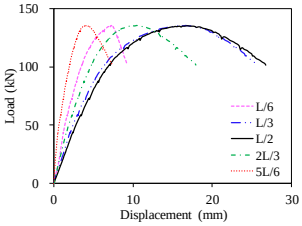

(e) ST-8-A-300-3.0

Fig. 9 Displacement-load curves of arches with damage at the arch end

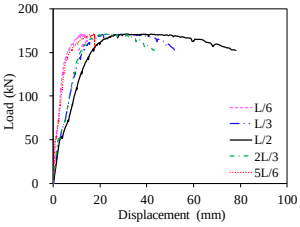

(a) ST-8-D-200-2.0

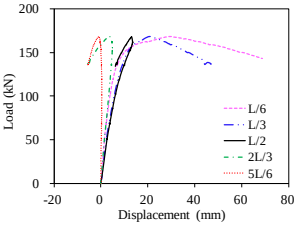

(b) ST-8-D-200-3.0

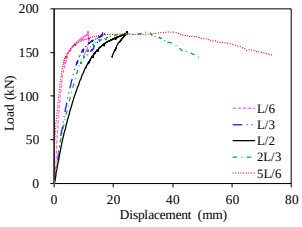

(c) ST-8-D-100-3.0

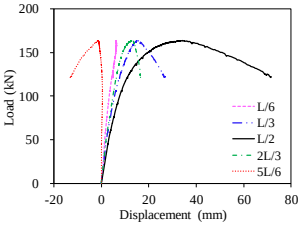

(d) ST-8-D-300-3.0

Fig. 10 Displacement-load curves of test specimens

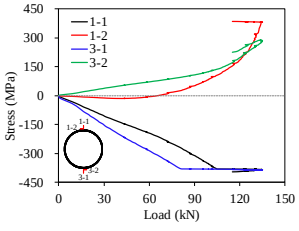

(a) A-A section

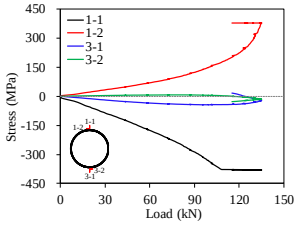

(b) B-B section

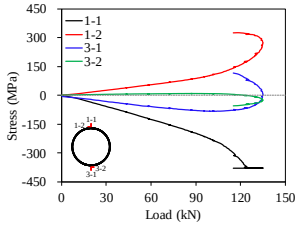

(c) C-C section

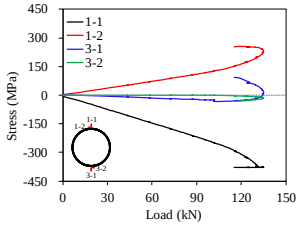

(d) D-D section

Fig. 11 Stress-load curves of specimen 6

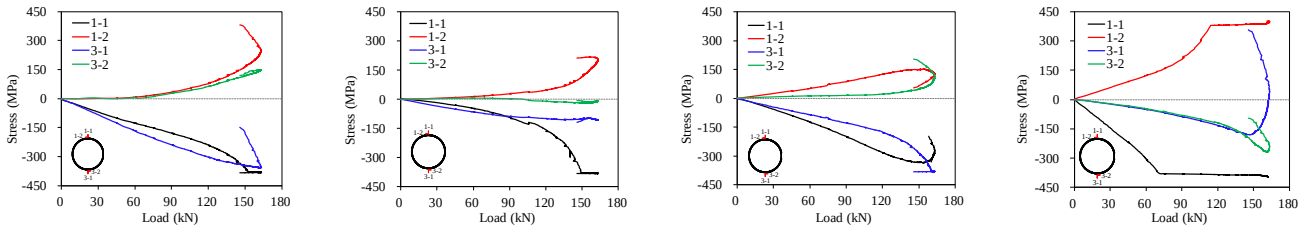

(a) A-A section (b) B-B section (c) C-C section (d) D-D section

Fig. 12 Stress-load curves of specimen 10

and depth at its left end and in Fig. 12 for specimen 10 having the largest damage length and depth at its crown, where the section labels A-A, B-B, C-C, and D-D are refereed to Fig. 5(b) and the stresses are derived from the measured strain based on the stress-strain curves in Fig. 3.

It can be seen from Fig. 11 that when the load is smaller than 80.4 kN, the stress increases linearly with an increase of the load. The blue curve in Fig. 11(a) indicates that the bottom of the left end of the arch of specimen 6 begins to yield at the load of 80.4 kN, while the black curves in Figs. 11(a) and (b) show that the top of sections A-A and B-B begins to yield at the load of 105 kN. When the applied load reaches 120 kN, the top of the sections C-C and D-D begins to yield (the black curves in Figs. 11(c) and (d)). Subsequently, the arch fails due to large plastic deformations.

It can be seen from Fig. 12 that for specimen 10, yielding onsets on the top of the arch crown (the point 1-1 in section D-D, the black curve in Fig. 12(d)) at the load of 72.4 kN while yielding starts on the top of the sections A-A and B-B at the load of 150 kN (the black curves in Figs. 12(a) and (b)). When the applied load reaches 162.1 kN, the bottom of the section C-C starts to yield (the blue curve in Fig. 12(c)). Subsequently, the arch fails due to large plastic deformation.

It can also be seen from Figs. 11 and 12 that even in the elastic stage, the longitudinal normal stresses vary over the cross-section indicating the arches are subjected to combined axial compressive and bending actions due to initial geometric imperfections and vertical deformations although a linear elastic analysis for a perfect undeformed parabolic arch under a vertical uniform load over the entire span produces axial uniform compression in the arch without bending.

3.4 Strength

The maximum value of the load of the *v*-*P* curves is defined as the strength (P_u) of the arch. When the strength of a specimen is reached, the further increase of displacements is associated with a decrease of the load until failure of the specimen. The test results for the strength of specimens are compared with the corresponding finite element (FE) results in Table 4.

It can be seen from Table 4 that the strength of damaged arches (specimens 2-10) is much smaller than that of the undamaged arch (specimen 1). It can also be seen that the strength of arches with local damages at their end (specimens 2-6) is generally smaller than that of arches with local damages at their crown (specimens 7-10), which indicates that damages at the arch end have more significant effects on the strength of the arch than damages at the arch crown.

4. Finite element analysis and comparison

4.1 Finite element model

4.1.1 Material properties

A finite element (FE) model for damaged steel tubular arches is formulated by using ANSYS (ANSYS 2014) and it is used to assess the remaining in-plane strength of the damaged arches.

Table 4 Measured strength and comparison with the FE results

No.	Specimen label	Measured value (kN)	Calculated value (kN)	Relative error
1	ST-8	190.3	182.6	-4.15%
2	ST-8-A-200-1.0	168.9	165.8	-1.84%
3	ST -8-A-200-2.0	150.9	147.7	-2.12%
4	ST -8-A-200-3.0	137.1	142.2	3.72%
5	ST -8-A-100-3.0	141.6	144.6	2.12%
6	ST -8-A-300-3.0	135.2	137.4	1.63%
7	ST -8-D-200-2.0	171.1	168.6	-1.46%
8	ST -8-D-200-3.0	167.9	161.7	-4.29%
9	ST -8-D-100-3.0	173.6	165.2	-4.84%
10	ST -8-D-300-3.0	163.5	160.6	-1.77%

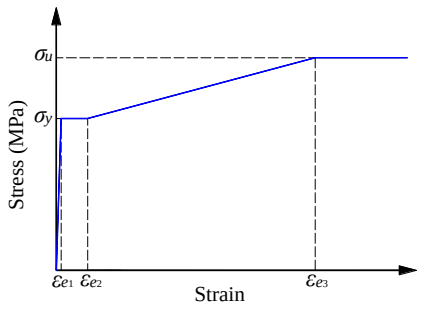

Fig. 13 Stress-strain curve of steel

The stress (σ) vs. strain (ε) model of Han *et al*. (2007) for the tubular steel shown in Fig. 13 is used, where σ_y and σ_u represent the yield and ultimate stresses of the steel respectively, and σ_y = 375.2 MPa and σ_u = 542.0 MPa are adopted, the strain corresponding to the yield stress is $\varepsilon_{e1} = 1.5\varepsilon_e$ with $\varepsilon_e = 0.8\,\sigma_y/E_s$, the steel hardening onset strain $\varepsilon_{e2} = 10\varepsilon_{e1}$, and the strain corresponding to the ultimate stress $\varepsilon_{e3} = 100\varepsilon_{e1}$. The initial Young's modulus of the steel is assumed as E_s = 1.91×10^5 MPa and the strain hardening modulus E_h = 0.79×10^3 MPa. It is noted that when the FE model is used to analyze the tested specimens, the measured values for σ_y and σ_u, the corresponding strains, E_s and E_h are assigned to the FE model.

4.1.2 Element description

In order to investigate the nonlinear behaviour of the steel tube, the 3-D beam element 188 of ANSYS is used for modeling. The beam 188 element is a 3D finite strain straight beam with 2 nodes and 7 degrees of freedom including three translation degrees of freedom and three rotation degrees of freedom and one degree of freedom for warping. Because there is no warping deformation for circular tubes, the degree of freedom for warping is suppressed. After a careful mesh convergence study, an appropriate mesh density is identified and 82 beam elements with 83 nodes are used to establish the FE model for the steel tubular arches.

4.1.3 Geometrical imperfections and residual stress

For the FE models used in parametric analysis and assessment equation establishment, the initial antisymmetric and symmetrical geometric imperfections are considered and they are given by

$$v_{0a} = v_{0m}\, sin\frac{2z\pi}{L} \quad \text{and} \quad v_{0s} = v_{0m}\, cos\frac{z\pi}{L} - \frac{L}{2} \le z \le \frac{L}{2} \tag{1}$$

respectively, where L is the span of the arch, z is the longitudinal coordinate of the cross-section, and the maximum value of the initial imperfection is v_{0m} = S/500.

It is noted that when using the FE model to analyze the test specimens, the measured initial geometric imperfections are assigned to the FE model.

In addition, the residual stresses of Lin and Guo (2009) shown in Fig. 14 are also assigned to the FE model.

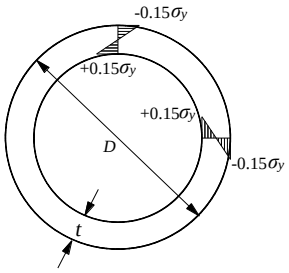

Fig. 14 Residual stress of steel tube

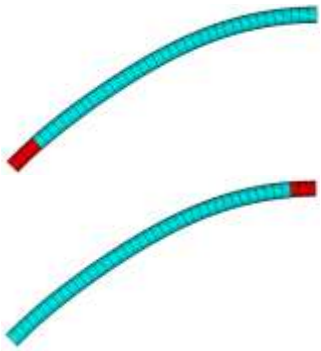

Fig. 15 Semi-structural FE model of steel tubular arch specimen

4.1.4 Damage simulation

The damages at the arch ends or arch crown are modeled by proper reduction of the outer radius of the steel tube. In the damaged region, the outer radius and thickness of the section of beam 188 element is properly reduced as shown in Fig. 15. In the figure, the red elements represent the damaged region. The damage parameters including the damage location, the damage length and the damage depth are considered in the FE model.

4.1.5 Implementation of FE model

To implement the material nonlinearity with the FE model, the Von Mises yield criterion, the Kinematic hardening rule, and the Bauschinger effect are adopted in association with the stress-strain curve shown in Fig. 13. To implement the nonlinear elastic-plastic analysis with the FE model, an arc-length method is employed for the increment-iterative nonlinear analysis in a displacement controlled fashion. Both ends of the arch model are fully fixed, and in order to prevent the out-of-plane displacement, the lateral and torsional degrees of freedom of all nodes are fully restrained.

4.2 Analytical results and comparison analysis

4.2.1 Displacement analysis

In order to validate the FE model, the FE model was used to analyze the tested arches. For this, the geometric and material properties of the tested arches and measured initial geometric imperfections were assigned to the FE model and the load locations of the FE model are the same as those of the tested arches.

The FE results for the strength of the arch specimens are

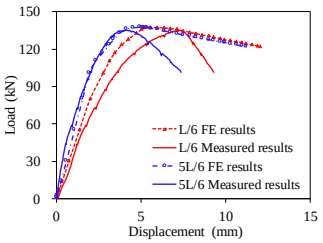

(a) $L/6$ and $5L/6$ Position

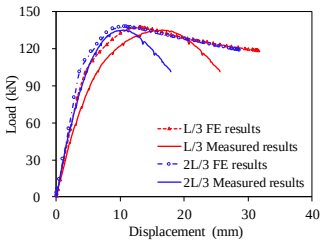

(b) $L/3$ and $2L/3$ Position

Fig. 16 Comparisons between test *v*-*P* curves and FE results of specimen 6

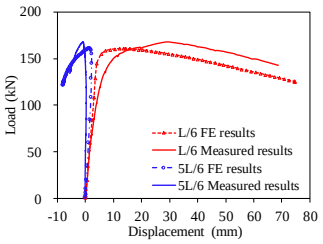

(a) $L/6$ and $5L/6$ Position

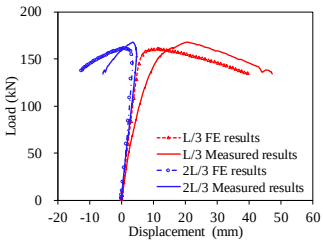

(b) $L/3$ and $2L/3$ Position

Fig. 17 Comparisons between test *v*-*P* curves and FE results of specimen 10

(a) Specimen 3 (asymmetric mode)

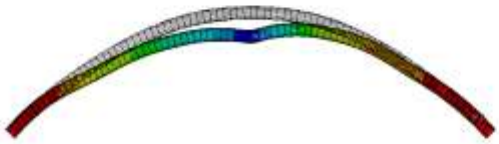

(b) Specimen 8 (symmetric mode)

Fig. 18 FE failure mode

compared with the test counterparts in Table 4. It can be seen that they agree with each other with relative differences less than 5%, which indicates the FE model is sufficiently accurate to predict the strength of damaged steel tubular arches.

The FE results of the *v*-*P* curves are compared with the corresponding test ones in Fig. 16 for the specimen 6 with a damage length of 300 mm and a damage depth of 3 mm at the left arch end. Fig. 16 shows that the FE and test results closely agree with each other until the strength of the arch is reached and the FE prediction for the strength also agree well with the test one.

The FE results for the *v*-*P* curves are compared with their test counterparts in Fig. 17 for the specimen 10 with a damage length of 300 mm and a damage depth of 3 mm at the arch crown.

Again, it can be seen from Fig. 17 that the FE results closely agree with the test ones until the strength of the arch is reached and the FE prediction for the strength also agree well with the test one. This further validate that the FE model can be used to predict the strength of damaged steel tubular arches.

4.2.2 Failure mode analysis

To further justify the accuracy of the FE model, the failure of specimens 3 and 7 shown in Fig. 6 was analyzed using the FE model. The FE results for failure modes of specimens 3 and 7 are shown in Fig. 18. It can be seen that specimen 3 fails in an asymmetric elastic-plastic buckling, while specimen 7 fails in an in-plane symmetric elastic-plastic buckling, which have excellent agreements with the test results in Fig. 6. It is found that the failure mode is dependent on the shape of in-plane initial geometric imperfections of the arch. The asymmetric initial geometric imperfections of specimen 3 leads to its asymmetric failure mode, while the symmetric in-plane initial geometric imperfections of specimen 7 leads to its symmetric failure mode. These are consistent with the test results. For further justification of the FE model in predicting the failure mode of damaged steel tubular arches, the failure modes obtained by the FE model are compared with tested ones of all 10 specimens in Table 3, which shows that they agree with each other very well.

5. Parametric studies

The verified FE model can be used to perform parametric studies to investigate the influence of various damage factors on the strength of steel arches and to generate sufficient number of FE results for the strength of damaged steel tubular arches. The FE results together with

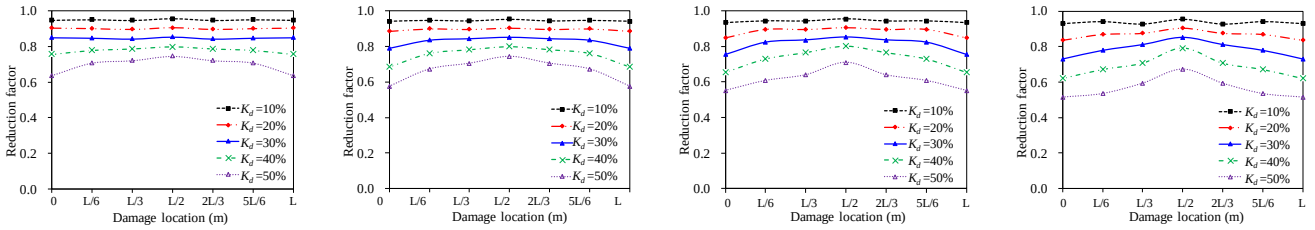

(a) K_ℓ = 8% (b) K_ℓ = 12% (c) K_ℓ = 16% (d) K_ℓ = 20%

Fig 19 Strength of arches with different damage locations

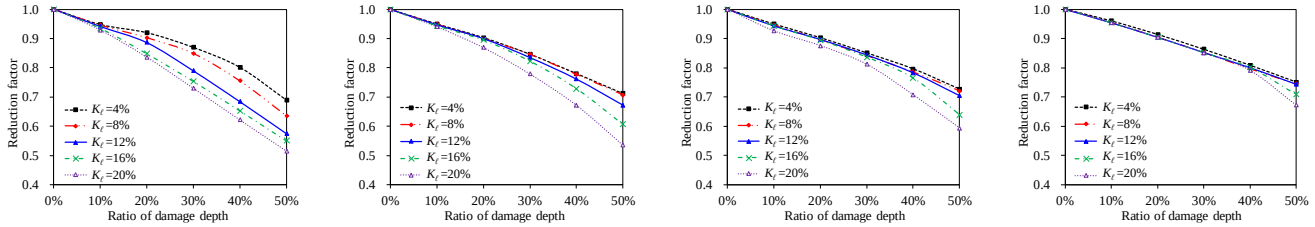

(a) Damaged at arch end (b) Damaged at L/6 (c) Damaged at L/3 (d) Damaged at L/2

Fig. 20 Strength of arches with different damage depths

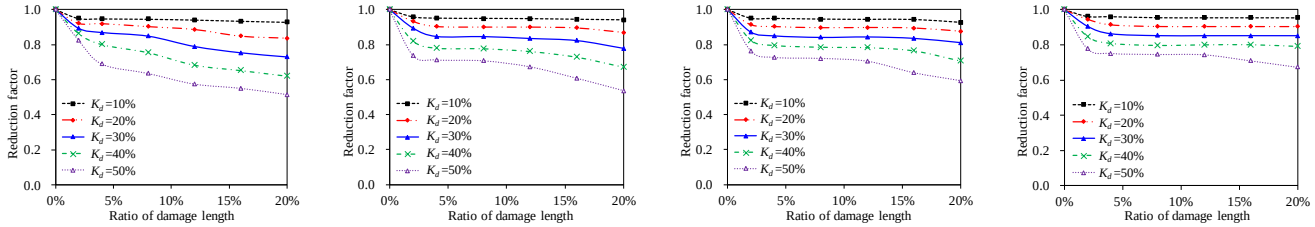

(a) Damaged at arch end (b) Damaged at L/6 (c) Damaged at L/3 (d) Damaged at L/2

Fig. 21 Strength of arches with different damage lengths

the test results are used to propose equations for assessing the remaining strength of damaged steel tubular arches. For this, the influences of the following parameters on the strength of damaged steel tubular arches are investigated: (1) damage location, (2) damage length, (3) damage depth.

5.1 Damage location

The effects of the damage location on the strength of damaged steel arches are investigated in this section using the FE model. The FE results for the strengths of damaged steel tubular arches with different damage locations are shown in Fig. 19 as the variations of the reduction factor with the damage location where K_ℓ and K_d are damage length and depth ratios respectively. The ratio K_ℓ is defined as the ratio of the damage length to the full length of the arch while K_d is defined as the ratio of the damage depth to the thickness of the steel tube.

It can be seen that when the damage length ratio K_ℓ is the same and the damage depth ratio K_d < 20%, the strengths of arches having different damage locations are almost the same. This indicates that in this case, the damage location has little effect on the strength of the damaged arches. However, when $K_d \geq$ 20%, the reduction effect of the damage location on the strength increases with an increase of K_d. It can also be seen from Fig. 19 that the reduction of the strength of the damaged arches gradually decreases as the damage location moves from the arch crown to the arch end. The damage at the arch end has more significant reduction effects on the strength than the damage at the arch crown. For example, when K_d = 50% and K_ℓ = 20%, the reduction factor for the strength of the arch with damages at its crown is 0.67, while the reduction factor for the arch with damages at its end is 0.52.

5.2 Damage depth

The effects of the damage depth on the strength of damaged steel arches are herein investigated using the FE model. The FE results for the strength of the steel arches with different damage depths are shown in Fig. 20 as the variations of the reduction factor with the ratio of damage depth. It can be seen that the damage depth has significant reduction effects on the strength of the arch. For the same damage location, the strength is reduced linearly with the increase of the damage depth. Comparisons of the strengths of damaged arches at different locations shown in Figs. 20(a)-(d) demonstrate that the reduction effect of the

damage length on the strength become more significant as the damage location moves from the arch crown ($L/2$) to the arch end.

5.3 Damage length

Effects of the damage length on the strength of arches are shown in Fig. 21 as the FE results for the variations of reduction factor with the damage length. It can be seen that when the damage length ratio increases from zero to 2%, the strength of arch decreases rapidly. After that, the reduction rate of the strength is getting slow with a further increase of the damage length. When the damage depth is small (K_d = 10% - 30%), the further increase of the damage length beyond 5% of the arch length does not decrease the strength of the arch very much.

6. Proposed assessment equation for remaining strength

6.1 Remaining strength of demaged arches in uniform compression

It can be seen from the experimental and FE study in this paper that strengths of damaged steel tubular arches are lower than those of undamaged arches. To ensure the safety of damaged arches, it is demanded to assess the remaining strength of the damaged arches. It is known that a general vertical load would produce axial compressive and bending actions of a damaged parabolic arch. To develop equations for assessing the remaining strength of a parabolic arch, it is essential to establish the equation for assessing the remaining strength of the arch under uniform axial compression. The uniform compression can nominally be produced by a vertical load uniformly distributed over the full arch span. Hence, a uniform vertical load over the full arch span is applied to the verified FE model to investigate remaining strengths of damaged parabolic steel tubular arches in uniform compression. The FE results for the remaining strengths of 114 damaged steel arches under the axial compression are obtained. For comparison, the strengths of 18 undamaged arches are also obtained using the FE model. These FE results for the remaining strength together with the test results for the 10 arch specimens are used to develop the equation for the remaining strength of damaged arches under uniform axial compression.

However, no design equations for the strength of steel arches are available in the current design codes. Hence, the design equations for the strength of steel members in uniform compression provided in GB50017 (2017) and Eurocode 3 (2004) are herein used to assess the remaining strength of damaged parabolic steel tubular arches in uniform compression after properly considering the effects of local damages. For this, the effective cross-section considering local damages is proposed to be used in determining the axial stiffness, bending stiffness and the squash load of the cross-section.

Based the 10 test and 132 FE results, the assessment equation for the remaining in-plane strength N_{ac} of damaged steel tabular arches under uniform axial compression is proposed as

$$\varphi = \frac{N_{ac}}{N_Y} = \frac{N_{ac}}{\sigma_y A} \le 1 \tag{2}$$

where φ is the reduction factor and it is expressed as the function of the normalized slenderness $\lambda_n^{'}$ of damaged arches as

$$\varphi = \begin{cases} 1 - \alpha_1 \lambda_n^{'2} & \lambda_n^{'} < 0.215 \\ \dfrac{1}{2\lambda_n^{'2}}\left[\left(\alpha_2 + \alpha_3\lambda_n^{'} + \lambda_n^{'2}\right) - \sqrt{\left(\alpha_2 + \alpha_3\lambda_n^{'} + \lambda_n^{'2}\right)^2 - 4\lambda_n^{'2}}\right] & \lambda_n^{'} \ge 0.215 \end{cases} \tag{3}$$

in the Chinese code for steel structures GB50017 (2017), and as

$$\varphi = \frac{1}{0.5\left[1 + \alpha(\lambda_n^{'} - 0.2) + \lambda_n^{'2}\right] + \sqrt{0.5^2\left[1 + \alpha(\lambda_n^{'} - 0.2) + \lambda_n^{'2}\right]^2 - \lambda_n^{'2}}} \tag{4}$$

in Eurocode 3 (2004), where the normalized slenderness λ'_n for damaged arches is given by

$$\lambda_n^{'} = \sqrt{\frac{N_Y^{'}}{N_{acr}}} = \sqrt{\frac{\sigma_y A_{eff}}{N_{acr}}} \tag{5}$$

in which the affective area A_{eff} is the area of the damaged cross-section, σ_y is the yield strength of the steel, N_{acr} is the in-plane buckling axial compression of the damaged parabolic arches under uniform compression. For non-shallow parabolic arches, N_{acr} can be calculated as (Dou *et al*. 2014).

$$N_{acr} = \frac{q_{acr} L}{2\sin\alpha_{L/2}} \tag{6}$$

where L is the span of the arch, $\alpha_{L/2}$ is the angle between the tangent direction of the arch axis at the arch end and the horizontal direction, and q_{acr} is the critical buckling load of the damaged parabolic arch given in Timoshenko and Gere (1961).

$$q_{acr} = K_\gamma \frac{EI_{eff}}{L^3} \tag{7}$$

where K_γ is a factor related to the rise-to-span ratio $\gamma = f/L$ where f is the rise of the arch (Timoshenko and Gere 1961), which are given in Table 5.

For shallow parabolic arches (γ < 0.1) which can be treated as circular arches, the buckling axial compression is calculated using the equation proposed by Pi and Bradford (2008) as

$$N_{acr} = \begin{cases} (0.36 + 0.0011\lambda^2)\dfrac{\pi^2 EI}{(0.35S)^2} & 9.87 \le \lambda \le 18.6 \\ \left(0.6 + 0.4\sqrt{1 - 3.109\dfrac{\pi^4}{\lambda^2}}\right)\dfrac{\pi^2 EI}{(0.35S)^2} & \lambda > 18.6 \end{cases} \tag{8}$$

where λ is a modified slenderness defined by

$$\lambda = \frac{2f}{r_x} \tag{9}$$

Table 5 Values of K_γ for parabolic arches of constant cross section under a vertical uniform load

γ	0.1	0.2	0.3	0.4	0.5	0.6	0.7	0.8
K_γ	60.7	101	115	111	97.4	83.8	59.1	43.7

When Eqs. (2) and (3) are used to assess the remaining strength of damaged arches based on GB50017 (2017), the curve *b* of GB50017 (2017) with coefficients α_1 = 0.65, α_2 = 0.965, and α_3 = 0.3 is recommended.

When Eqs. (2) and (4) are used, the curve *b* of Eurocode 3 (2004) with the imperfection coefficient α =0.34 is recommended.

The predictions of remaining strengths of damaged arches by Eqs. (2)-(3) or (2)-(4) are compared with the test and FE results in Fig. 23(a) where the reduction factor and modified slenderness of the FE results are calculated based the gross undamaged cross-sections. It can be seen that when the gross undamaged cross-section is used to calculate the reduction factor and modified slenderness, the equations (2)-(3) or (2)-(4) can conservatively estimate the strengths of undamaged arches, but significantly overestimate the strength of damaged arches as shown in Fig. 23(a). When the reduction factor and modified slenderness of the test and FE results are calculated based the effective cross-sections, i.e. the damaged cross-section for damaged arches and the gross-section for undamaged arches, the comparisons are shown in Fig. 23(b). It can be seen that the proposed equations can provide conservative assessments for remaining strengths of both undamaged and damaged arches.

6.2 Design strength in combined bending and compression

In the engineering practice, arches subjected to pure uniform compression are rare and in the most cases, arches are subjected to combined axial compressive and bending actions produced by external loading. Hence, equations for assessing the remaining strength of damaged arches under axial compressive and bending actions are much needed. The strengths of arches subjected to combined bending and axial compressive actions are related to a number of factors, such as the damaged location, damaged depth, rise-to-span ratio, the slenderness, residual stresses, initial in-plane geometric imperfections, loading conditions and so on. Therefore, it is difficult to develop simple and accurate equations for assessing remaining strengths of damaged arches under general loading. In this paper, instead, a lower bound interaction equation is proposed for assessment of remaining strengths of damaged parabolic steel tubular arches under combined bending and compression based on the FE results.

The equation for assessing remaining in-plane strengths for a damaged parabolic steel arch subjected to combined bending and axial compressive actions is then proposed as

$$\frac{N^*}{\beta\alpha_{an}N_{ac}^{'}}+\frac{M^*}{\beta\alpha_{am}M_p^{'}}\le 1 \tag{10}$$

where N^* and M^* are the maximum axial compression and moment obtained by a first-order in-plane elastic analysis for damaged arches; $N_{ac}^{'}$ is the remain in-plane strength of a damaged steel tubular arch in uniform compression given by Eq. (2); $M_p^{'}$ is the full plastic moment of the effective cross-section given by

$$M_p^{'}=\sigma_y Z_p^{'} \tag{11}$$

with σ_y being the yield strength of the steel and $Z_p^{'}$being the plastic modulus of the effective cross-section; and α_{an} and α_{am} are the modification factors for the in-plane strength, and β is the modification factor of damage degrees.

The modification factor α_{am} accounts for the non-uniform distribution of bending moments over the arch length, while the modification factor α_{an} accounts for the non-uniform distribution of axial compressive forces over the arch length. The values of α_{an}, α_{am} and β are given in Table 6 for damaged parabolic steel tubular arches having fixed ends.

In Table 6, K_d is the ratio of damage depth, and $\lambda_s=\frac{S}{r_x}$ is the slenderness ratio of the arch with *S* being the axial length of the arch and r_x being the radius of gyration of the cross-section.

The predictions of the proposed interaction given by Eq. (10) are compared in Figs. 24 and 25 with the results of the verified FE model for the arches under the four load cases

(a) Calculated with gross cross-section (b) Calculated with effective cross-section

Fig. 23 Remaining strength of damaged arches

Table 6 Factors for in-plane strength of fixed parabolic arches

Load cases		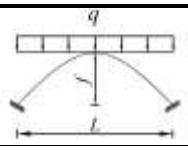	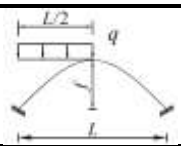	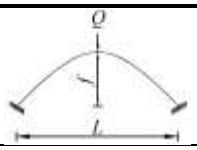	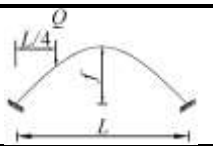
α_{an}		1.0	1.0	1.1	1.1
α_{am}	$\gamma \leq 0.1$	3.0	1.8	$1.2+\frac{30}{\lambda_s}$	$1.2+\frac{15}{\lambda_s}$
	$\gamma > 0.1$	$3.84-\frac{\lambda_s}{125}$	$2.04-\frac{\lambda_s}{125}$	$1.2+\frac{30}{\lambda_s}$	$1.2+\frac{15}{\lambda_s}$
β		$1+(K_d)^2$	$1+(K_d)^2$	$1+(K_d)^2$	$1+(K_d)^2$

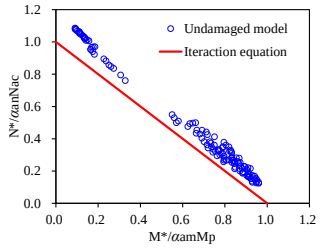

Fig. 24 In-plane strength of fixed arches without damages using gross area

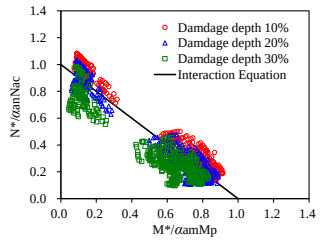

Fig. 25 In-plane strength of fixed arches with damages using gross area

listed in Table 6. The FE results consists of 1620 damaged arches (405 arches for each load cases), and 144 undamaged arches (36 arches for each load cases).

In Figs. 24 and 25, the gross undamaged cross-sections are used to calculate the axial compression capacity N_{ac} of the arch and the in-plane full plastic moment M_p of the cross-section.

It can be seen that the interaction Eq. (10) based on the gross cross-section can predict the strength of undamaged steel arches very well (Fig. 24), but significantly overestimates the strength of damaged steel arches (Fig. 25).

When the effective damaged cross-section is used to determine the axial compression capacity N_{ac} of the arch and the in-plane full plastic moment M_p of the cross-section, the comparisons of the predictions of the proposed Eq. (10) with the FE results are shown in Fig. 26. It can be seen that the interaction Eq. (10) provides good lower bound predictions for the remaining strengths of damaged steel tubular arches. It can be concluded that the effective cross-

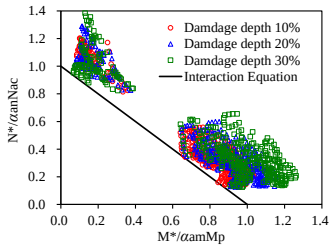

Fig. 26 In-plane strength of fixed arches with damages using effective area

section of the damaged arches should be used in the assessment of their remaining strengths.

7. Conclusions

Experimental studies of effects of local damages on the in-plane elastic-plastic buckling response and remaining strength of fixed parabolic steel tubular arches under a vertical five-point loading were presented in this paper. A FE model for damaged parabolic steel tube arches was formulated and validated by the test results and it was then used for further investigations of effects of the various parameters on the in-plane elastic-plastic buckling behaviour of damaged arches. It was found that the local damage significantly reduces the remaining in-plane elastic-plastic buckling strengths of steel tubular arches. It was also found that the remaining strengths with local damages at the arch end are lower than those with local damages at the arch crown. In addition, test results showed that the reduction effect of the depth of the local damage is more significant than that of the length of the local damage. It was further found that the failure mode shape of a damaged steel arch is very much dependent on the shapes of the initial geometric imperfections of the arch.

The test and FE results were used to investigate remaining strengths of damaged fixed steel tubular arches in nominal uniform axial compression. The equations for assessing the remaining strengths of damaged steel tubular arches were developed based on the FE and test results. It has been shown that curve *b* of the codes GB50017 (2017) and Eurocode 3 (2004) for steel members in uniform axial compression can be used for predicting the remaining in-

plane strength of damaged parabolic steel tubular arches as long as the effective cross-section considering damages and the elastic in-plane buckling load of damaged parabolic arches in uniform compression are used in calculating the normalized slenderness of the arches.

Based on a large number of FE results, an interaction equation was proposed for assessing remaining in-plane strengths of damaged steel tubular arches that are subjected to the combined bending and axial compression. The interaction equation considers the effect of damages on the remaining strengths of arches by using the effective cross-section to calculate the remaining in-plane axial compression strength of the damaged arch and the full plastic moment of the damaged cross-section. In addition to the modification factors for the in-plane axial compression strength of the arch and the full plastic moment of the cross-section, a modification factor for damage degrees was introduced. Comparisons of the interaction equation with the large number of FE results showed that the proposed interaction equation provides good lower bound predictions for the remaining in-plane strength of damaged steel arches that are subjected to the combined bending and axial compressions.

Acknowledgments

This research is financially supported by the National Natural Science Foundation of China (No. 51678169, 51878188), Pearl River S&T Nova Program of Guangzhou (No. 201710010147), and Technology Planning Project of Guangzhou (No. 201807010021).

References

Ahn, J., Kim, I.T., Kainuma, S. and Lee, M.J. (2013), "Residual shear strength of steel plate girder due to web local corrosion", *J. Constr. Steel Res.*, **89**(5), 198-212. https://doi.org/10.1016/j.jcsr.2013.07.008.

ANSYS (2014), Multiphysics, Release 14.5, Ansys Inc., Canonsburg, PA, USA.

Appuhamy, J.M.R.S., Ohga, M., Kaita, T., Fujii, K. and Dissanayake, P.B.R. (2011), "Development of analytical method for predicting residual mechanical properties of corroded steel plates", *Int. J. Corros.*, 1-10. https://doi.org/10.1155/2011/385083.

Appuhamy, J.M.R.S., Ohga, M., Chun, P. and Dissanayake, P.B.R. (2013), "Role of corrosion and earthquakes on degradation of dynamic behaviour of steel bridge plates", *J. Civ. Eng. Sci.*, **2**(1), 7-14.

Bradford, M.A. and Pi, Y.L. (2004), "Design of steel arches against in-plane instability", *Int. J. Appl. Mech. Eng.*, **9**(1), 37-45. https://doi.org/10.1016/B978-008044017-0/50011-1.

Cai, J.G., Feng, J., Chen, Y. and Huang, L.F. (2009), "In-plane elastic stability of fixed parabolic shallow arches", *Sci. China Ser. E: Technol. Sci.*, **52**(3), 596-602. https://doi.org/10.1007/s11431-009-0057-9.

Dou, C., Guo, Y.L., Pi, Y.L. and Zhao, S.Y. (2014), "Flexural-torsional buckling and ultimate resistance of parabolic steel arches subjected to uniformly distributed vertical load", *J. Struct. Eng.*, **140**(10), 04014075. https://doi.org/10.1061/(ASCE)ST.1943-541X.0000997.

Dou, C., Guo, Y.L., Zhao, S.Y. and Pi, Y.L. (2015), "Experimental investigation into flexural-torsional ultimate resistance of steel circular arches", *J. Struct. Eng.*, **141**(10), 04015006. https://doi.org/10.1061/(ASCE)ST.1943-541X.0001240.

Dou, C., Guo, Y.F., Jiang, Z.Q., Gao, W. and Pi, Y.L. (2018), "In-plane buckling and design of steel tubular truss arches", *Thin-Wall. Struct.*, **130**, 613-621. https://doi.org/10.1016/j.tws.2018.06.024.

Eurocode 3 (2004), Design of steel structures, Part 1-1: General rules and rules for buildings, EN 1993-1-1, European Committee for Standardization; Brussels, Belgium.

GB50017 (2017), Code for design of steel structures. Ministry of Construction of the People's Republic of China; Beijing, P.R. China.

Guo, Y.L., Chen, H., Pi, Y.L. and Bradford, M.A. (2016), "In-plane strength of steel arches with a sinusoidal corrugated web under a full-span uniform vertical load: Experimental and numerical investigations", *Eng. Struct.*, **110**(3), 105-115. https://doi.org/10.1016/j.engstruct.2015.11.056.

Hadjoannou, M., Douthe, C. and Gantes, C. (2011), "Influence of residual stresses induced by cold curving on the resistance of I-Section steel members", *Eurosteel 2011*, 729-734.

Han, L.H., Zhao, X.L. and Tao, Z. (2001), "Tests and mechanics model for concrete-filled SHS stub columns, columns and beam-columns", *Steel Compos. Struct.*, **1**(1), 51-74. https://doi.org/10.12989/scs.2001.1.1.051.

Han, L.H., Yao, G.H. and Tao, Z. (2007), "Performance of concrete filled thin-walled steel tubes under pure torsion", *Thin-Wall. Struct.*, **45**(1), 24-36 .https://doi.org/10.1016/j.tws.2007.01.008.

Huang, Y.H. (2010), "Mechanism and effect of arch rib disease and suspender replacement for concrete-filled steel tube arch bridges", Ph.D. Dissertation; South China University of Technology, Guangzhou, China. [In Chinese]

Kainuma, S., Jeong, Y.S. and Ahn, J.H. (2015), "Stress distribution on the real corrosion surface of the orthotopic steel bridge deck", *Steel Compos. Struct.*, **18**(6), 1479-1492. https://doi.org/10.12989/scs.2015.18.6.1479.

Kaita, T., Appuhamy, J., Ohga, M. and Fujii, K. (2012), "An enhanced method of predicting effective thickness of corroded steel plates", *Steel Compos. Struct.*, **12**(5), 379-393. https://doi.org/10.12989/scs.2012.12.5.379.

Kim, I.T., Lee, M.J., Ahn, J.H. and Kainuma, S. (2013), "Experimental evaluation of shear buckling behaviors and strength of locally corroded web", *J. Constr. Steel Res.*, **83**(2), 75-89. https://doi.org/10.1016/j.jcsr.2012.12.015

Lin, B. and Guo, Y.L. (2009), "In-plane stability behavior and application of parabolic arches under pure compression", *J. Build. Struct.*, **30**(3), 103-111. [In Chinese]

Liu, A.R., Huang, Y.H., Fu, J.Y., Yu, Q.C and Rao, R. (2015), "Experimental research on stable ultimate bearing capacity of leaning-type arch rib systems", *J. Constr. Steel Res.*, **114**(11), 281-292. https://doi.org/10.1016/j.jcsr.2015.08.011

Liu, A.R., Lu, H.W., Fu, J.Y. and Pi, Y.L. (2017), "Lateral-torsional buckling of fixed circular arches having a thin-walled section under a central concentrated load", *Thin-Wall. Struct.*, **118**, 46-55. https://doi.org/10.1016/j.tws.2017.05.002

Mateus, A.F. and Witz, J.A. (1998), "On the post-buckling of corroded steel plates used in marine structures", *RINA Trans*, **140**, 165-183.

Pi, Y.L. and Bradford, M.A. (2004), "In-plane strength and design of fixed steel I-section arches", *Eng. Struct.*, **26**(3), 291-301. https://doi.org/10.1016/j.engstruct.2003.09.011.

Pi, Y.L. and Trahair, NS (1999), "In-plane buckling and design of steel arches", *J. Struct. Eng.*, **125**(11), 1291-1298. https://doi.org/10.1061/(ASCE)0733-9445(1999)125:11(1291).

Pi, Y.L., Bradford, M.A. and Tin-Loi, F. (2008), "In-plane strength

of steel arches,. *Adv. Steel Constr.*, **4**(4), 306-322.
Rahbar-Ranji, A. (2013), "Elastic buckling strength of corroded steel plates", *Sādhanā,* **38**(1), 89-99. https://doi.org/10.1007/s12046-013-0116-6.
Rahgozar, R. (2009), "Remaining capacity assessment of corrosion damaged beams using minimum curves", *J. Constr. Steel Res.*, **65**(2), 299-307. https://doi.org/10.1016/j.jcsr.2008.02.004
Rahgozar, R., Sharifi, Y. and Malekinejad, M. (2010), "Buckling capacity of uniformly corroded steel members in terms of exposure time", *Steel Compos. Struct*., **10**(6), 475-487. https://doi.org/10.12989/scs.2010.10.6.475.
Sakimoto, T., Yamao, T. and Komatsu, S. (1979), "Experimental study on the ultimate strength of steel arches", *Proc. Jpn. Soc. Civ. Eng*., **286**, 139-149. https://doi.org/10.2208/jscej1969.1979.286_139.
Sharifi, Y. and Paik, J.K. (2011), "Ultimate strength reliability analysis of corroded steel-box girder bridges", *Thin-Wall. Struct.*, **49**(1), 157-166.
Silva, J.E., Garbatov, Y. and Soares, C.G. (2013), "Ultimate strength assessment of rectangular steel plates subjected to a random localised corrosion degradation", *Eng. Struct.,* **52**(9), 295-305. https://doi.org/10.1016/j.engstruct.2013.02.013
Timoshenko, S.P. and Gere, J.M. (1961), *Theory of Elastic Stability*, (2th Ed.), McGraw-Hill Book Company, Inc., New York.
Yang, Z.C., Huang, Y.H., Liu, A.R., Fu, J.Y. and Wu, D. (2019) "Nonlinear in-plane buckling of fixed shallow functionally graded grapheme reinforced composite arches subjected to mechanical and thermal loading", *Appl. Math. Model.*, **70**, 315-327. https://doi.org/10.1016/j.apm.2019.01.024

BU